Fundamental Research xxx (xxxx) xxx

Contents lists available at ScienceDirect

Fundamental Research

journal homepage: http://www.keaipublishing.com/en/journals/fundamental-research/

Article

The implementation of ecological protection in Inner Mongolia has slowed down grassland degradation

Haojun Zheng [a,b,c], Yao Huang [d], Wen Zhang [b], Changqing Song [a], Qing Zhang [b], Wenjuan Sun [d], Yongqiang Yu [b], Lijun Yu [b], Haigang Li [e], Cunhou Zhang [f], Wenfang Jiang [a], Xinyue Yang [a], Guocheng Wang [a,g,h,*]

[a] Faculty of Geographical Science, Beijing Normal University, Beijing 100875, China
[b] State key Laboratory of Atmospheric Boundary Layer Physics and Atmospheric Chemistry, Institute of Atmospheric Physics, Chinese Academy of Sciences, Beijing 100029, China
[c] College of Earth and Planetary Sciences, University of Chinese Academy of Sciences, Beijing 100029, China
[d] State Key Laboratory of Vegetation and Environmental Change, Institute of Botany, Chinese Academy of Sciences, Beijing 100093, China
[e] Inner Mongolia Key Laboratory of Soil Quality and Nutrient Resources/Key Laboratory of Agricultural Ecological Security and Green Development at Universities of Inner Mongolia Autonomous Region, Inner Mongolia Agricultural University, Hohhot 010018, China
[f] Inner Mongolia Ecology and Agrometeorology Center, Hohhot 010018, China
[g] State Key Laboratory of Earth Surface Processes and Resource Ecology, Beijing Normal University, Beijing 100875, China
[h] Center for Geodata and Analysis, Beijing Normal University, Beijing 100875, China

ARTICLE INFO

Article history:
Received 27 February 2024
Received in revised form 14 September 2024
Accepted 8 October 2024
Available online xxx

Keywords:
Ecological protection and restoration
Fractional vegetation cover
Grassland degradation index
Inner Mongolia
Normalized difference vegetation index
Remote sensing

ABSTRACT

The Inner Mongolia grassland has been facing critical degradation. To combat this issue, China has launched a series of ecological restoration programs since the early 2000s to promote the recovery of degraded grasslands (e.g., the Beijing–Tianjin Wind/Sand Source Control Program, the Grazing Withdrawal Project, and the Ecological Compensation Policy). However, the long-term effects of these measures on the recovery of the Inner Mongolia grassland still need further evaluation. To quantitatively assess the grassland degradation status and dynamics, we utilized long-term remote sensing datasets (GIMMS NDVI and MODIS NDVI) from 1982 to 2020 to calculate the fractional vegetation cover (FVC, the ratio of vegetation canopy's vertical projection area to the unit area) and grassland degradation index (GDI, the ratio of average FVC during peak growing season to historical optimum FVC). Results showed that across the study region, the average FVC was 42% over the past four decades, with degraded grassland (GDI < 0.9) accounting for 84.6% of the total area. Noteworthy spatial differences were observed. Specifically, study region to the west of 115°E had an average FVC of 20.7% with 98.2% areas exhibiting a degraded state. By contrast, study region to the east had an average FVC of 57.7% with 68.5% areas experiencing degradation. Over time, the proportion of degraded grassland generally decreased, particularly in the past two decades. However, approximately 3/4 of the grassland remained degraded in the last decade (2011–2020). Although degraded grassland is recovering, grassland degradation remains serious, especially in the west of 115°E, where 80.8% of the grassland was moderately and severely degraded (GDI < 0.6) in the last decade. Our findings suggest that while the implementation of ecological protection measures in Inner Mongolia has slowed down grassland degradation, the persisting degradation underscores the necessity of region-specific grassland protection and restoration.

1. Introduction

Grassland ecosystems cover approximately 40% of the Earth's surface and play crucial roles, including supporting rich biodiversity, regulating climate, alleviating soil erosion, and providing resources for livestock [1]. However, grassland degradation is a globally widespread issue, affecting around 49% of the world's grasslands to some extent [2]. Moreover, in China, approximately 90% of natural grasslands are in a state of degradation, leading to significant reductions in grassland productivity and soil carbon storage [3].

Grassland degradation is broadly defined as a process of retrogressive ecosystem succession resulting from overexploitation, characterized by fragmented vegetation interspersed with patches of bare soil [4], specifically manifested as decreased vegetation coverage, reduced

* Corresponding author.
E-mail address: wanggc@bnu.edu.cn (G. Wang).

https://doi.org/10.1016/j.fmre.2024.10.006

Please cite this article as: H. Zheng, Y. Huang, W. Zhang et al., The implementation of ecological protection in inner Mongolia has slowed down grassland degradation, Fundamental Research, https://doi.org/10.1016/j.fmre.2024.10.006

aboveground biomass, changes in native populations, and reduced soil fertility [3,5]. Grassland degradation is normally caused by a combination of multiple drivers, including overgrazing, eutrophication, land conversion to forestry and crops, land abandonment, invasive species, extreme climate, and changes in fire regimes, which can be generally summarized as human activities and climatic factors [2]. In China, human activities (e.g., overgrazing), are considered as the primary factors for grassland degradation [6,7]. However, a recent study indicated that in the middle-south Inner Mongolia, climatic variation is more likely to cause grassland degradation compared to overgrazing [8], necessitating region-specific restoration strategies for degraded grasslands.

To combat grassland degradation, rehabilitation measures such as harrowing, sowing, fertilization and grazing management have been widely adopted across the globe [9,10]. Among these measures, grazing exclusion is the most widely adopted measure in northern China [11] and has been shown to effectively increase vegetation coverage, biomass, and soil fertility compared to continuous grazing, aiding in the recovery of degraded grasslands [12].

The Inner Mongolia grassland, a critical component of the Eurasian grasslands, is acknowledged as one of the most continuous, diverse, and representative temperate ecological systems worldwide [13]. It has also been experiencing degradation attributed to climate change and human activities, such as overgrazing and mineral overexploitation [8]. To halt such degradation, the Chinese government has launched a series of ecological restoration programs such as the Beijing–Tianjin Wind/Sand Source Control Program (BTWSSC) since 2001, the Grazing Withdrawal Project (GW) since 2003, and the Ecological Compensation Policy (EC) since 2011 (Supplemental Fig. S1) [14,15]. Over the past decade, 45.5 billion RMB has been invested in Inner Mongolia to support these restoration measures (http://www.xinhuanet.com/politics/2022-06/17/c_1128750321.htm). According to the data from the Inner Mongolia Statistical Yearbook (Supplemental Table S1; http://tj.nmg.gov.cn/), the area of fenced grassland, on average, was 137,561 km^2 (26.7% of the whole grassland area in Inner Mongolia, hereafter the same) over the period 2000–2004, and 298,110 km^2 (58.0%) over the period 2016–2020, respectively. In a more recent study, Huang et al. [16] found that hay production in China's grasslands exhibited a notable increase from 2005 to 2017 at a rate of 2.97 Tg DW a^{-1} (1 Tg = 10^9 kg; DW denotes dry weight) (Fig. S2a). This substantial increase could be primarily attributed to grassland restoration initiatives, including grazing exclusion (Fig. S2b). Moreover, field scale investigations have clearly shown that ecological restoration measures can effectively alleviate or even reverse grassland degradation by enhancing grassland productivity, species diversity, and carbon storage [17,18]. At the regional scale, Zhang et al. [19] also reported a marked improvement in plant growth over the past 21 years based on remote sensing data from 2000 to 2020. These studies generally focus on small areas or have short time scales. To date, there is a lack of quantitative assessment on the spatiotemporal changes in grassland degradation at reasonably large spatial and temporal scales, considering the impacts of both climate change and ecological restoration activities and their complex interactions.

Remote sensing technology offers image data with multiple temporal and spatial resolutions and has the advantages of wide coverage and long monitoring time, providing strong support for large-scale grassland vegetation monitoring [20]. Specifically, the remote sensing-based normalized difference vegetation index (NDVI) can be utilized to assess specific evaluation indices for grassland growth conditions, with fractional vegetation cover (FVC) being one of the most widely used index [21]. FVC is the ratio of the total land area covered by the vertical projection of the vegetation canopy to the unit area, indicating the extent of terrestrial vegetation cover, which serves as a valuable indicator of the degree and quality of grassland degradation [22]. Meanwhile, the grassland degradation index (GDI) can also be derived from the long-term FVC data, serving as an effective indicator for assessing grassland degradation situations [23,24].

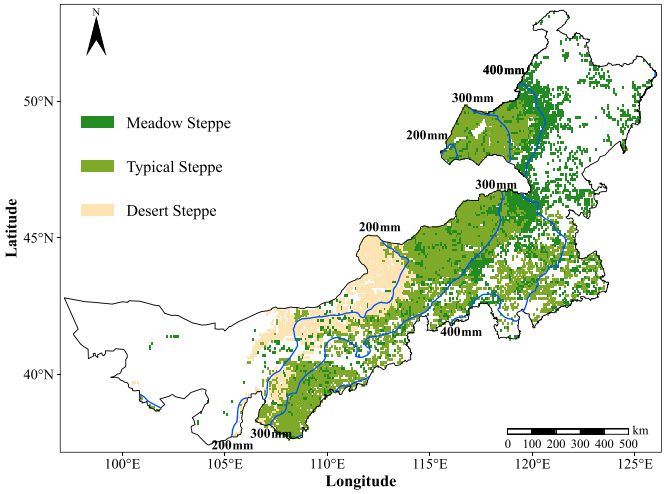

Fig. 1. Spatial distribution of the Inner Mongolia grassland. The blue lines represent rainfall isoclines. The map is based on the standard map with approval number GS (2024) 0650 from the Ministry of Natural Resources of the People's Republic of China. The base map boundaries remain unmodified.

Though there is sparse evidence that ecological restoration programs promoted the recovery of degraded grasslands [25,26], the long-term effects of these ecological protection on the recovery of the Inner Mongolia grassland still need further evaluation. Therefore, our study aims to fill this gap by evaluating the effectiveness of ecological protection measures in the Inner Mongolia grassland by comparing changes in grassland degradation conditions before and after the implementation of these measures. Specifically, using long-term (1982–2020) remote sensing datasets, we first analyzed the spatiotemporal variations in the FVC based on the relationship between FVC and NDVI. The trends in grassland degradation at different degraded levels were then identified over the last four decades. We expect that our findings in this paper could serve as the basis for policymaking in region-specific grassland protection and restoration.

2. Materials and methods

2.1. Study area

Inner Mongolia is located in northern China, spanning from 97° 12′ to 126° 04′ E and 37° 24′ to 53° 23′ N. This region's total grassland area is 51.4 million hm^2 [27], accounting for 17.5% of China's grassland area. Meadow steppe, typical steppe, and desert steppe account for 29.9%, 53.1%, and 17.0% of the total grassland in Inner Mongolia, respectively (Fig. 1). The region is markedly continental, with a predominantly temperate climate in most areas [28]. The mean annual temperature (MAT) varies greatly spatially, ranging from −5 to 9 °C [29]. The mean annual precipitation (MAP) ranges from 50 to 500 mm, while the annual evaporation (AP) amount ranges from 500 to 3,000 mm [30]. Inner Mongolia has a fragile ecological environment located in arid and semi-arid regions. Due to the impacts of climate change and human activities, most of the Inner Mongolia grassland has experienced substantial degradation since the 1960s [31].

2.2. Data sets

2.2.1. Normalized difference vegetation index data

To study the grassland degradation conditions over a long-term period (i.e., past 40 years), two NDVI datasets, i.e., Global Inventory Modeling and Mapping Study (GIMMS) and Moderate Resolution Imaging Spectroradiometer (MODIS) products, were used and integrated to generate a longer time series of a combined dataset (see

Section 2.3.1). Here, the long-sequence (1981–2015) GIMMS NDVI data (version 3 g.v1), with a temporal resolution of 15 days and a spatial resolution of 8 km, was obtained from the National Oceanic and Atmospheric Administration-Advanced Very High-Resolution Radiometer (NOAA-AVHRR) series data [32,33]. The MODIS NDVI data, covering the period 2000–2020 with 16-day temporal resolution and 1 km spatial resolution, was acquired from the National Aeronautics and Space Administration (NASA) [34]. Both NDVI datasets (GIMMS and MODIS) have undergone preprocessing steps, including geometric correction, radiometric correction, and atmospheric correction, to rectify geometric distortions [33,35]. As data for January 2000 was missing in the MODIS NDVI data, the corresponding month's mean value from 2001 to 2020 was used as a substitute. To minimize influences from clouds, non-vegetation elements, atmospheric conditions, and solar zenith angles, we employed the Maximum Value Composite (MVC) method for both datasets [36]. This method was used to calculate the monthly maximum NDVI, and NDVI values < 0 were excluded from the statistical analysis.

2.2.2. Meteorological data

Gridded monthly temperature and precipitation at a spatial resolution of 1 km for the study period (i.e., 1982–2020) were sourced from the National Tibetan Plateau Data Center (TPDC; https://data.tpdc.ac.cn/). This dataset was generated for the region of China using the Delta downscaling approach [37], which incorporated the global 0.5-degree climate dataset from the Climatic Research Unit (CRU) and the high-resolution climate dataset from WorldClim [38]. The MAT and MAP were then calculated for each pixel in the study region using the monthly datasets.

2.3. Data processing and analysis

2.3.1. Integration of GIMMS and MODIS NDVI data

The GIMMS NDVI time series covers the period 1982–2015, while the MODIS NDVI time series spans from 2000 to 2020 [32-34]. In order to effectively utilize both datasets and study the changes in FVC and GDI over a longer period (1982–2020), we chose to integrate these two sets and extend the GIMMS NDVI dataset to cover the 2016–2020 period. Given that the GIMMS and MODIS NDVI data originate from different sensors, possessing distinct spectral bands, temporal ranges, spatial resolutions, and other characteristics, it is imperative to integrate the two datasets for the ease of subsequent analysis and to check their spatiotemporal consistency [39].

In this study, the MODIS NDVI data was firstly resampled to 8 km to match the GIMMS NDVI data. These two datasets have a temporal overlap for the years 2000–2015. Consequently, a pixel-wise regression equation was constructed for the GIMMS and MODIS NDVI data from 2000 to 2015 using a simple linear regression model, where the MODIS NDVI was used as the independent variable and GIMMS NDVI as the dependent variable [40]. The applied formulas are as follows (Eq. 1):

$$G_i = a \times M_i + b \times \varepsilon_i \tag{1}$$

where G_i and M_i represent NDVI for the i month derived from the GIMMS and MODIS data, respectively. a and b are regression coefficients determined for each pixel. ε_i is the random error. The coefficient of determination (R^2) was utilized to evaluate the model's goodness of fit on each pixel, and the t-test was employed for hypothesis testing to ascertain the statistical significance of the model parameters.

In general, we found that the GIMMS and MODIS NDVI data are consistent in temporal variations of NDVI (Supplemental Fig. S3). The scatter plot demonstrates significant consistency ($R^2 = 0.93$, $p < 0.01$; Supplemental Fig. S4). Moreover, these two datasets across space are generally comparable in the study region (Supplemental Fig. S4). Then, the fitted regression equation (i.e., Eq. 1) extended the GIMMS NDVI data for 2016–2020, using the MODIS NDVI data from the same period as predictors. This established a long-term NDVI dataset for Inner Mongolia from 1982 to 2020, combining original GIMMS NDVI data for 1982–2015 and extrapolated data for 2016–2020 using Eq. 1.

2.3.2. Calculation of fractional vegetation cover

Following Gutman and Ignatov [41], we employed a semi-empirical relationship, known as the pixel dichotomy model, to derive the FVC from NDVI. The model postulates that the NDVI of a mixed pixel can be represented by (Eq. 2):

$$NDVI = FVC \times NDVI_{veg} + (1 - FVC) \times NDVI_{soil} \tag{2}$$

and the FVC derived by the NDVI as (Eq. 3):

$$FVC = \left(NDVI - NDVI_{soil}\right) / \left(NDVI_{veg} - NDVI_{soil}\right) \tag{3}$$

where FVC represents the vegetation coverage of the pixel to be calculated, and NDVI corresponds to the vegetation index of the same pixel. $NDVI_{soil}$ and $NDVI_{veg}$ correspond to the NDVI values of bare soil pixels and fully vegetation-covered pixels, respectively. In theory, the values of $NDVI_{soil}$ and $NDVI_{veg}$ should be 0 and 1, respectively. However, due to noise points on the image and grayscale interference with NDVI, these values often exhibit anomalies and can vary in different regions and at different times [42]. As such, using fixed values is not ideal. Alternatively, in this study, the values for $NDVI_{soil}$ and $NDVI_{veg}$ are determined by capturing the NDVI values corresponding to the cumulative frequency in the confidence interval at 0.5% and 99.5% [43].

To further confirm the validity of the integrated new NDVI dataset, we also computed the FVC using the two datasets of GIMMS and MODIS across the overlapped period of 2000–2015 for each pixel. The comparison indicated that the FVC calculated from two NDVI datasets had high temporal (Fig. S5) and spatial consistency (Fig. S6), with > 90% and around 60% of the pixels having an R^2 higher than 0.4 and 0.6, respectively (Fig. S6).

It has been reported that the peak growing season (July-September) is the optimal period for vegetation growth, particularly in northern China [40]. Using the extended GIMMIS NDVI data and calculated FVC data, we also demonstrated that FVC during July–September is generally the highest in a year across different latitudinal areas in the study region (Fig. S7). Therefore, we selected the average value of FVC during July-September as the representative annual FVC. This choice mitigates potential biases or uncertainties introduced by remote sensing identification in different periods. For instance, distinguishing between withered vegetation and bare soil in remote sensing applications is challenging due to their similar spectral characteristics [44]. To analyze the spatiotemporal variations of FVC within the study area, following Liu et al. [42], we categorized FVC into five levels, i.e., low, medium-low, medium, medium-high, and high coverage (Table S2).

2.3.3. Assessing the magnitude and significance of the temporal changes in fractional vegetation cover

We first used the Theil-Sen Median trend analysis [45] to evaluate the temporal variations of FVC. This method calculates the median of a sequence, effectively reducing interference caused by noise. It is robust to measurement errors and outliers, computationally efficient, and widely used in the analysis of long-term trends in meteorology and hydrology [46]. The trend is defined as (Eq. 4):

$$trend = Median\left[\left(x_j - x_i\right)/(j - i)\right], 1 \le i < j \le n \tag{4}$$

where n represents the number of years studied, and x_i and x_j represent the FVC values of the years i and j, respectively. A positive trend indicates an overall increase in FVC over time, while a negative trend indicates an overall decrease.

Considering the fact that the Theil-Sen Median trend analysis does not provide a significance test for the trend, we further adopted the Mann-Kendall test approach [47] in this study. Compared to other parametric tests, the Mann-Kendall test does not assume a specific distribution for the data and is suitable for conducting significance tests on long

time series [48]. The test statistic S is calculated using the following formula (Eq. 5):

$$S = \sum_{i=1}^{n-1} \sum_{j=i+1}^{n} sgn\left(x_j - x_i\right) \tag{5}$$

where n is the ordinal of data in the series, $(x_j - x_i)$ is the difference between the FVC values of adjacent years and $sgn()$ is a sign function, which can be calculated as (Eq. 6):

$$sgn\left(x_j - x_i\right) = \begin{cases} +1, & x_j - x_i > 0 \\ 0, & x_j - x_i = 0 \\ -1, & x_j - x_i < 0 \end{cases} \tag{6}$$

The standardized test statistic Z is computed as (Eq. 7):

$$Z = \begin{cases} (S-1)/\sqrt{Var(S)}, & x_j - x_i > 0 \\ 0, & x_j - x_i = 0 \\ (S+1)/\sqrt{Var(S)}, & x_j - x_i < 0 \end{cases} \tag{7}$$

where $Var(S)$ is calculated as (Eq. 8):

$$Var(S) = n(n-1)(2n+5)/18 \tag{8}$$

The statistic Z obeys the standard normal distribution with a mean of zero and a variance of one. At a given significance level α, if $|Z| > u_{(1-\alpha/2)}$, the null hypothesis at α significance level will be rejected, which indicates the time series has a significant temporal trend.

2.3.4. Calculation of grassland degradation index

Despite the lack of a unified evaluation standard for grassland degradation in the academic community, many previous studies have already tried to use the GDI to assess grassland conditions [23,24]. The GDI is defined as the ratio of the actual FVC of grassland to its FVC in the non-degraded state. However, it is crucial to acknowledge that for a given pixel, the FVC of grasslands in the non-degraded stage cannot be directly obtained due to data limitations. To address this issue, we employed the space-for-time substitution approach, which has been widely applied [49,50]. This method involves utilizing data from regions with similar climatic conditions across relatively large spatial and temporal scales to estimate the FVC of the target pixel in the non-degraded stage. Technically, this is an effective method to approximate the grassland FVC in the non-degraded state given the absence of historical data.

In this study, taking the maximum FVC of the grassland for each pixel from 1982 to 2020 grouped by different climate types (characterized by different combinations of MAT and MAP) as a baseline, we further determined the GDI to characterize the degradation status of the grassland over time in the study region. Here, following Wiesmair et al. [51], we categorized the degradation into four levels using the determined GDI: non-degraded ($0.8 \leq GDI \leq 1$), lightly degraded ($0.6 \leq GDI < 0.8$), moderately degraded ($0.4 \leq GDI < 0.6$), and severely degraded ($0 \leq GDI < 0.4$). In each pixel, GDI was calculated as follows (Eq. 9):

$$GDI = FVC_{real}/FVC_{max} \tag{9}$$

where GDI represents the grassland degradation index of the evaluated pixel, while FVC_{real} and FVC_{max} represent the respective pixel's actual and maximum fractional vegetation cover, respectively. In determining FVC_{max}, we first calculated the average MAT and MAP for each year from 1982 to 2020 in each pixel. We then sorted and divided these MAT and MAP into 100 groups, respectively, resulting in 10,000 different climate types. Here, pixels with the same climate type of MAT and MAP were further grouped together. Within each climate type group, the pixel with the highest FVC between 1982 and 2020 is identified as FVC_{max} for all the pixels in the corresponding climate type group.

2.3.5. Residual trend (RESTREND) analysis

Vegetation growth is influenced not only by climatic factors but also by human activities. To isolate the impacts of climate change and human activities on vegetation dynamics, following Evans and Geerken [52], we further conducted a residual trend analysis at each pixel. Specifically, a Multivariate Linear Regression (MLR) was fitted, treating the observed FVC as the dependent variable and two climatic variables (MAT and MAP) as the independent variables. The residuals were further acquired from the difference between the observed and the MLR-predicted FVC. In the residual analysis, if the residual trend over time is insignificant ($p > 0.05$), the FVC variations can be explained by climatic factors. On the other hand, significant positive and negative trends indicate promoting and adverse impacts of human activities, respectively. All data processing and analyzing were performed in Python (version 3.10.10).

3. Results

3.1. Temporal changes in fractional vegetation cover

Table 1 shows the area proportions of FVC change in the Inner Mongolia grassland across two periods: 1982–2000 and 2001–2020. Between 1982 and 2000, 12.6% and 1.1% of the grassland showed a significant ($p < 0.05$ and $p < 0.01$) increase and decrease in FVC, respectively. By contrast, 25.7% of the grassland showed a significant increase in FVC over the period 2001–2020, approximately twice as much as that over the period 1982–2000. Meanwhile, 1.7% of the whole region experienced a significant decrease in FVC.

The FVC in the Inner Mongolia grassland generally increased from 1982 to 2020 (Fig. 2a), while the trend in FVC with time was not significant ($p > 0.1$) either in the whole grassland (Fig. 2a) or in different grassland types (Fig. S8). However, the FVC increase trend over the period 2001–2020 was significant ($p < 0.05$) for the whole grassland at a rate of 0.27% a^{-1} (Fig. 2a). The increase rate (0.35% a^{-1}) in the typical steppe (Fig. S8b) was higher than that (0.22% a−1) in the meadow steppe (Fig. S8a), which agreed with the FVC changes in Table 1.

It is noteworthy that the grassland in the west of 115°E, where the typical steppe and desert steppe dominate, showed a significant ($p < 0.05$) increase in FVC over the period 1982–2020 at a rate of 0.10% a^{-1} (Fig. 2b). The increase rate in the second period (0.27% a^{-1}) was higher than that in the first period (0.15% a^{-1}). However, the FVC trend in the east of 115°E grassland, where the meadow steppe and typical steppe dominate, was not significant ($p > 0.1$) (Fig. 2c). The mean value of FVC over the period 2011–2020 was generally higher than those in the other periods (Table S3). In comparison with the mean value of FVC over the period 1982–2010, the mean FVC in the last decade (2011–2020) significantly increased by 15.6% ($p < 0.001$) in the west of 115°E (1982–2010: 19.9% ± 2.0%; 2011–2020: 23.0% ± 3.0%) and by 5.3% ($p < 0.05$) in the east of 115°E (1982–2010: 56.9% ± 3.1%; 2011–2020: 59.9% ± 4.1%), respectively.

3.2. Spatial variations of fractional vegetation cover

In both the first (1982–1990) and the last (2011–2020) decades, the multi-year average FVC generally decreased from northeast to southwest (Fig. 3a,b). The regional average FVC was 41.4% ± 2.0% in the first decade and 44.2% ± 3.2% in the last decade (Table S3). Across these two periods, a shift from low to medium-low vegetation coverage generally occurred in the southwestern area, particularly in the typical steppe (Fig. 3a,b). Furthermore, the proportion of low vegetation coverage area in the typical steppe decreased from 17.5% in the first decade to 11.5% in the last decade, with a reduction of 34.3% (Fig. 3a,b). It is also noteworthy that the proportion of low vegetation coverage area in the desert steppe decreased by 10.5%, and that of medium-low vegeta-

Table 1
Area proportions of the grassland fractional vegetation cover (FVC) change and its significance across two time periods: 1982–2000 and 2001–2020.

Period	Grassland type	Trend	*p*-value		
			$p < 0.01$	$p < 0.05$	$p > 0.05$
1982–2000	Meadow steppe	< 0	0.8%	2.0%	35.6%
		= 0	–	–	0.4%
		> 0	7.4%	4.3%	49.5%
	Typical steppe	< 0	0.2%	0.3%	22.0%
		= 0	–	–	0.2%
		> 0	9.7%	5.9%	61.7%
	Desert steppe	< 0	0.1%	0.1%	13.7%
		= 0	–	–	1.0%
		> 0	1.1%	3.8%	80.2%
	Total	< 0	0.4%	0.7%	24.7%
		= 0	–	–	0.4%
		> 0	7.5%	5.1%	61.2%
2001–2020	Meadow steppe	< 0	2.1%	2.8%	21.2%
		= 0	–	–	0.4%
		> 0	15.0%	8.1%	50.4%
	Typical steppe	< 0	0.1%	0.1%	15.3%
		= 0	–	–	0.1%
		> 0	23.6%	9.0%	51.8%
	Desert steppe	< 0	0.1%	0.4%	31.3%
		= 0	–	–	0.8%
		> 0	4.2%	4.1%	59.1%
	Total	< 0	0.7%	1.0%	19.7%
		= 0	–	–	0.3%
		> 0	17.8%	7.9%	52.6%

Note: $p < 0.01$, $p < 0.05$, and $p > 0.05$ indicate highly significant, significant, and insignificant, respectively.

tion coverage area increased by 64.6% from the first to the last decade (Fig. 3a,b).

The area with FVC increasing over the period 1982–2000 was mainly distributed in the southwestern and southeastern parts (Fig. 4a, c). Across the whole region, the average linear trend of FVC was 0.12% a^{-1} during this period (Fig. 4a). Specifically, typical steppe had the largest increase in FVC (0.15% a^{-1}), followed by desert steppe (0.10% a^{-1}) and meadow steppe (0.07% a^{-1}).

Similar to that of the period 1982–2000, the increase in FVC was mainly distributed in the southwestern and southeastern regions over the period 2001–2020 (Fig. 4b). The FVC increase in the western part of the northeast region was also significant (Fig. 4b, d). Across the entire region, the linear trend of FVC from 2001 to 2020 was 0.27% a^{-1} (Fig. 4b). Typical steppe had the largest increase in FVC (0.35% a^{-1}), followed by meadow steppe (0.23% a^{-1}) and desert steppe (0.10% a^{-1}). It is noteworthy that the growth rates of different types of grasslands from 2001 to 2020 were generally higher than those corresponding to the period from 1982 to 2000 (Fig. 4a,b).

The slope-change trend of the grassland FVC between the two periods (i.e., 1982–2000 and 2001–2020) was calculated (Fig. 5). The area where grasslands continuously improved, primarily located in the southwest and southeast regions, accounted for 8.9% of the total grassland area. Grasslands that transitioned from a stable to an improving state, accounting for 16.6%, were mainly situated in the southwest and southeast, with a smaller portion in the northeast. However, a small proportion of grasslands (1.6%) remained in a deteriorating state in the period 2001–2020, mainly distributed in the northeastern region. Furthermore, 3.5% of the grasslands transitioned from an improving to a stable state, predominantly distributed in the central region.

3.3. Trends in grassland degradation over the last four decades

The proportion of degraded grassland in Inner Mongolia from 1982 to 2020 consistently exceeded 65% (Fig. S9), especially in the typical steppe and the desert steppe (Fig. 6). Across the entire grassland, there were pronounced spatial disparities in grassland degradation. Specifically, in the west of 115°E, the total proportion of moderately degraded (MD) and severely degraded (SD) grasslands averaged 88.2% ± 7.6%, and that of non-degraded (ND) grassland averaged 1.8% ± 2.1% over the period 1982–2020 (Fig. 7; Supplemental Table S4). By contrast, the total proportion of MD and SD grasslands averaged 29.0% ± 11.3%, and that of ND grassland averaged 31.5% ± 9.6% (Fig. 7; Table S4) in the east of 115°E at the same period.

Nevertheless, the recovery of the degraded grassland was evident over time. In the last decade (2011–2020), the MD and SD grasslands were significantly lower, and the ND grassland was significantly higher than those in other periods (Fig. 7; Table S4). Overall, the total proportion of MD and SD grasslands (47.4% ± 9.3%) decreased by 16.1% ($p < 0.01$), and that of ND grassland (24.4% ± 6.8%) increased by 44.4% ($p < 0.001$) in the last decade across the entire grassland when compared with the means (56.5% ± 7.6% for MD and SD grasslands; 16.9% ± 4.7% for ND grassland) over the period 1982–2010. The restoration of the degraded grassland, specifically the increase in non-degraded grassland area in the east of 115°E, was more pronounced than that in the west of 115°E (Fig. 7; Table S4). In the east of 115°E, the total proportion of MD and SD grasslands in the last decade (22.5% ± 11.6%) decreased by 27.9% ($p < 0.05$), that of ND grassland (39.1% ± 10.7%) increased by 44.4% ($p < 0.01$), while that of lightly degraded (LD) grassland (38.4% ± 4.2%) did not change, in comparison with the means (31.2% ± 10.4% for MD and SD grasslands; 28.8% ± 7.8% for ND grassland; 40.0% ± 4.5% for LD grassland) over the period 1982–2010 (Fig. 7; Table S4). By contrast, the total proportion of MD and SD grasslands (1982–2010: 90.7% ± 4.7%; 2011–2020: 80.8% ± 9.9%) decreased by 10.9% ($p < 0.001$), that of ND grassland increased from 0.8% ± 0.9% to 4.5% ± 2.4% ($p < 0.001$), and that of LD grassland increased from 8.5% ± 3.9% to 14.7% ± 7.7% ($p < 0.01$) in the west of 115°E (Fig. 7; Table S4).

Consistent with the changes in FVC (Fig. 2), the increase in ND grassland and the decrease in degraded grassland in the second period (2001–2020) were more pronounced than those in the first period (1982–2000). The proportion of the ND grassland significantly increased at a rate of 0.64% a^{-1}, and the total proportion of the MD and SD grasslands significantly decreased at a rate of 0.81% a^{-1} (Table 2). The proportion of the LD grassland increased significantly in the west of 115°E, but no

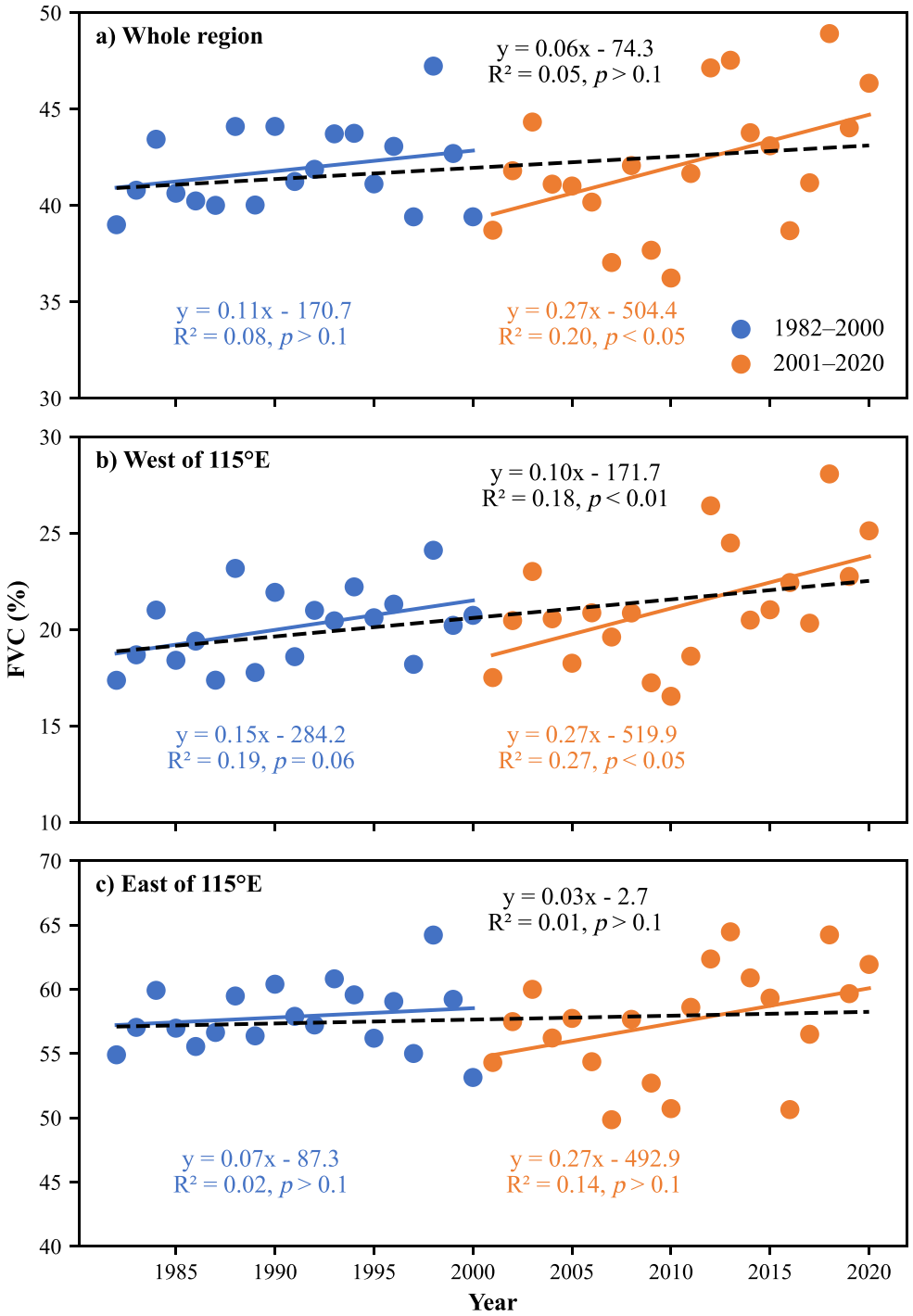

Fig. 2. Temporal variations in fractional vegetation cover (FVC) in the Inner Mongolia grassland during 1982–2020. (a) The whole grassland, (b) grassland in the west of 115°E, and (c) grassland in the east of 115°E.

significant changes were detected in the east of 115°E (Table 2). Note that the increase in the proportion of ND grassland and the decrease in the total proportion of MD and SD grasslands in the west of 115°E were significant over the period 1982–2020 (Table 2).

Although the recovery of the degraded grassland was evident over time, the current situation of grassland degradation is still serious, especially in the west of 115°E (Fig. 6b). Our results show that the proportion of degraded grassland in the last decade was 75.6% ± 6.8%, and the total proportion of MD and SD grasslands was 47.4% ± 9.3% across the whole region (Fig. 7; Table S4). Approximately 72% of the MD and SD grasslands were distributed in the west of 115°E (Fig. 6b).

3.4. Residual analysis

The linear regression analysis based on the FVC residuals revealed that the area with a significant ($p < 0.05$) positive trend increased from 8.8% during 1982–2000 (Fig. 8a) to 19.3% during 2001–2020 (Fig. 8b), indicating the overall positive effects of ecological restoration measures. This change was particularly pronounced in the southwestern region, where the area with a significant ($p < 0.05$) positive trend expanded considerably between the two periods. The observed trend aligns with the results shown in Table 1, which shows that the area with a significant increase in FVC during 2001–2020 (25.7%) is greater than that during

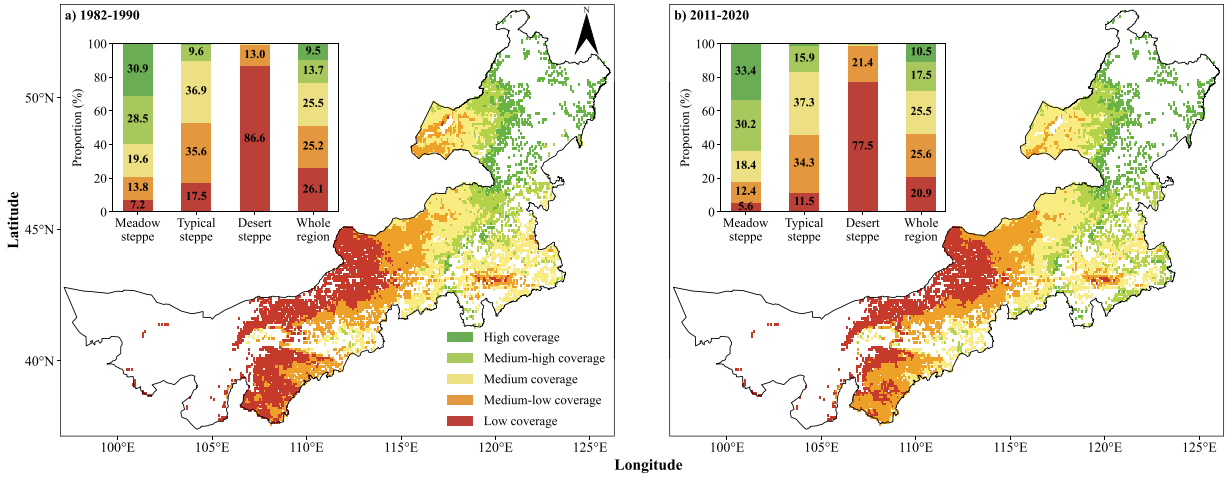

Fig. 3. Spatial distribution of fractional vegetation cover (FVC) in the Inner Mongolia grassland. (a) 1982–1990 and (b) 2011–2020. The grassland is categorized based on their FVC as follows: low coverage (0–20%), medium-low coverage (20%–40%), medium coverage (40%–60%), medium-high coverage (60%–80%), and high coverage (80%–100%). Inset bar charts show the proportions of different vegetation cover classification across different grassland types. Colors correspond to vegetation cover classification as indicated in the legend. The vegetation cover classification was calculated based on the average FVC for each of the two periods. The proportions of vegetation cover classification in the inset bar charts are calculated based on the average proportions of yearly vegetation cover classification over the same two periods. The map is based on the standard map with approval number GS (2024) 0650 from the Ministry of Natural Resources of the People's Republic of China. The base map boundaries remain unmodified.

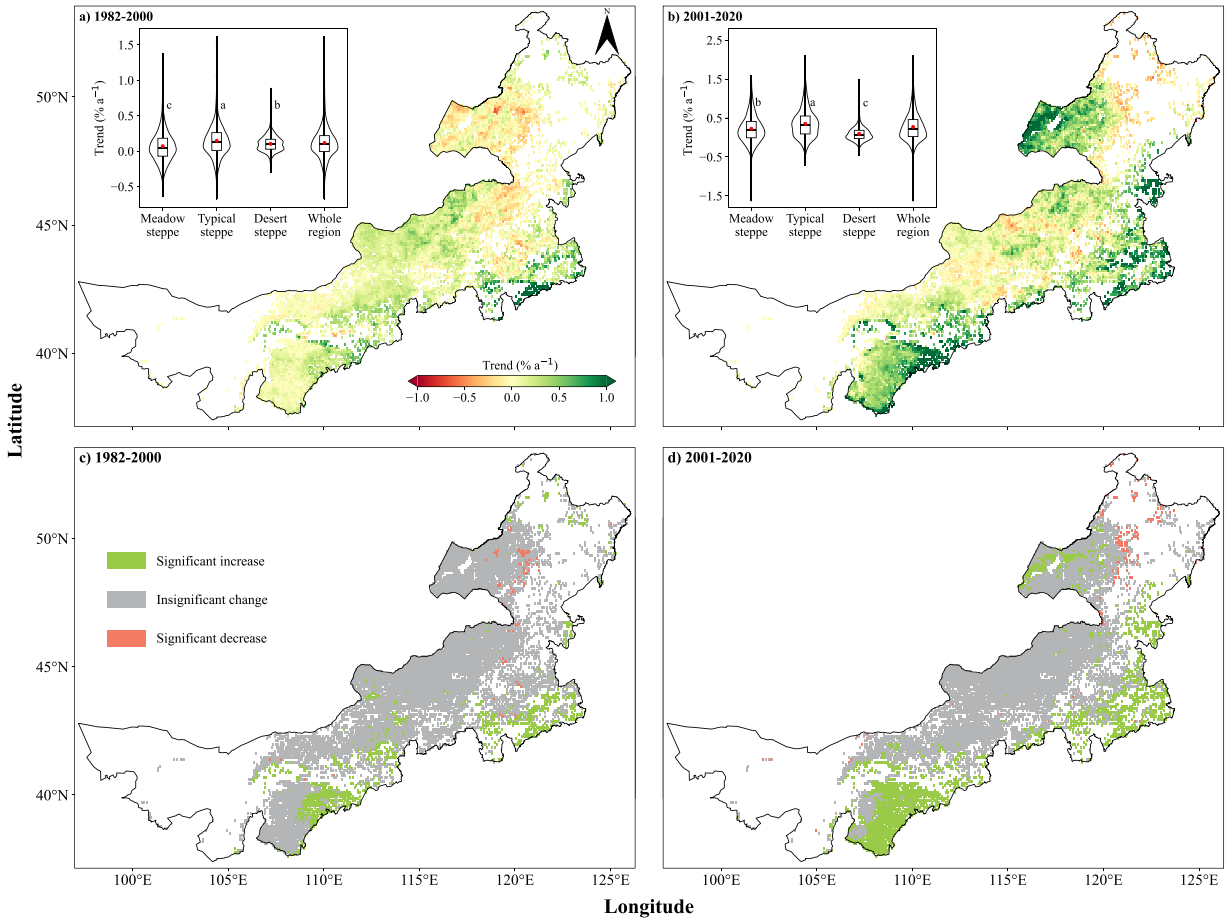

Fig. 4. Spatial trends of fractional vegetation cover (FVC) changes and their significance in the Inner Mongolia grassland. (a, c) 1982–2000 and (b, d) 2001–2020. Inset figures show the violin plot distribution of spatial trends across different grassland types. In the violin plot, the central black horizontal line of the box represents the median. The black horizontal lines on either side of the box indicate the upper quartile and lower quartile, while the vertical black lines at the top and bottom represent the maximum and minimum values. The red dots represent the mean. The violin plots accompanied by distinct characters and the significant trend exhibit statistical significance at the $p < 0.05$ level. The map is based on the standard map with approval number GS (2024) 0650 from the Ministry of Natural Resources of the People's Republic of China. The base map boundaries remain unmodified.

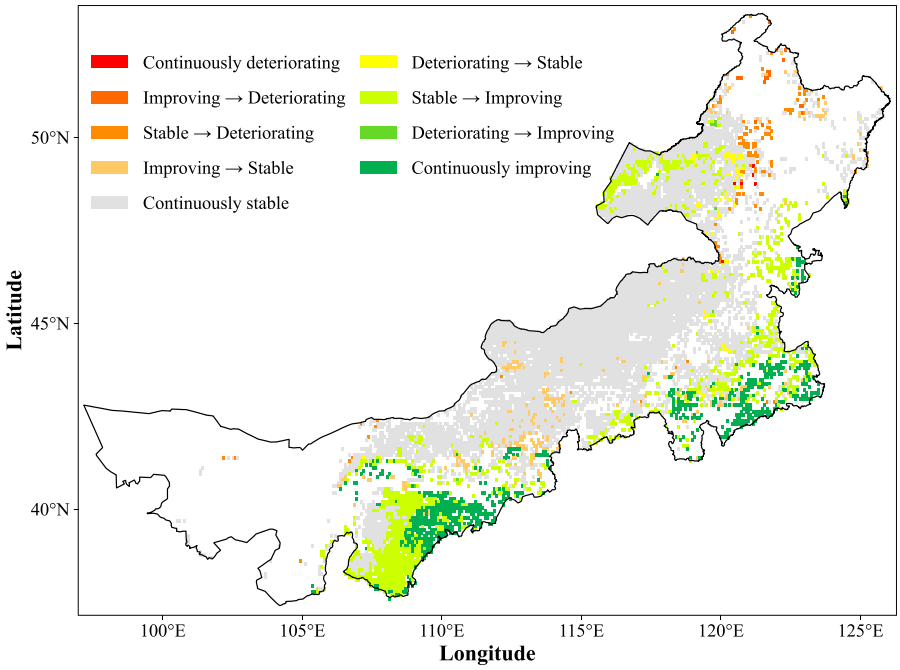

Fig. 5. Slope-change trend of fractional vegetation cover (FVC) in the Inner Mongolia grassland between 1982–2000 and 2001–2020. The criteria for judging the slope-change trend refers to Supplemental Table S5. The map is based on the standard map with approval number GS (2024) 0650 from the Ministry of Natural Resources of the People's Republic of China. The base map boundaries remain unmodified.

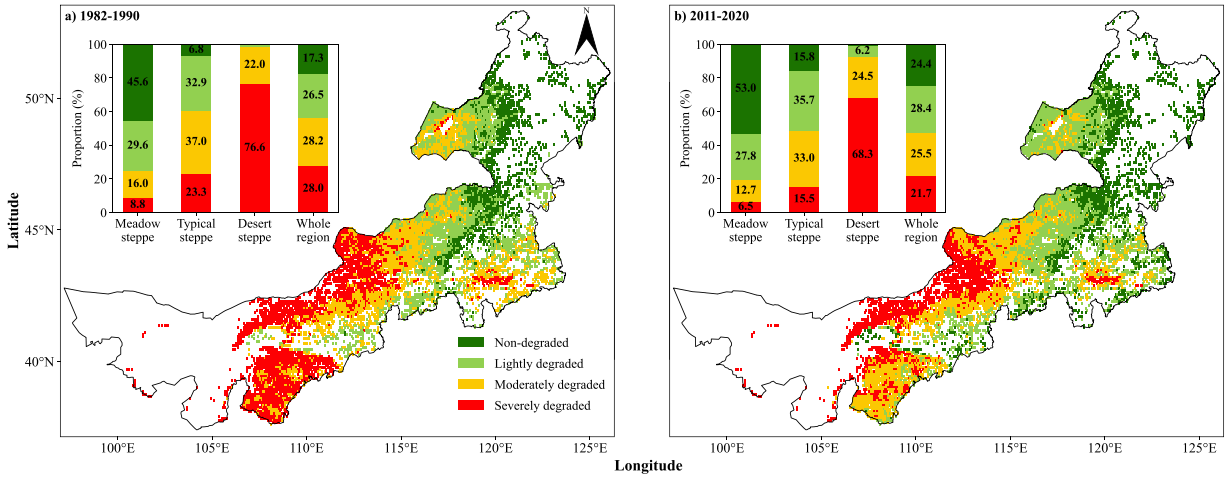

Fig. 6. Spatial distribution of grassland degradation condition in the Inner Mongolia grassland. (a) 1982–1990 and (b) 2011–2020. The grassland is categorized based on their grassland degradation index (GDI) as follows: severely degraded grassland (0–0.4), moderately degraded grassland (0.4–0.6), lightly degraded grassland (0.6–0.8), non-degraded grassland (0.8–1.0). Inset bar charts display the percentage of each degradation level for meadow steppe, typical steppe, desert steppe, and the total area. Colors correspond to degradation levels as indicated in the legend. The grassland degradation conditions in the figures are calculated based on the average GDI for each of the two periods. The proportions of grassland degradation condition in the inset bar charts are calculated based on the average proportions of yearly grassland degradation condition over the same two periods. The map is based on the standard map with approval number GS (2024) 0650 from the Ministry of Natural Resources of the People's Republic of China. The base map boundaries remain unmodified.

1982–2000 (12.6%). However, some regions in the northeast and central parts also exhibited significant ($p < 0.05$) decreasing trends during 2001–2020 (Fig. 8b), indicating that human activities may have intensified grassland degradation in these areas.

Notably, the increase in the positive trend was more evident in the typical steppe compared to other grassland types (Fig. 8; Table 1). Specifically, in the typical steppe, the proportion of area with a significant ($p < 0.05$) positive trend reached 25.1% during 2001–2020. However, it should be noted that the area with significant ($p < 0.05$) downward trend in parts of desert steppe became more widespread during 2001–2020 (Fig. 8b), with the proportion reaching 7.8%.

4. Discussion

Our study utilizes the longest record of remote sensing data available for Inner Mongolia to date. This extensive dataset facilitates the analysis of how ecological protection measures have impacted grassland restoration processes. Most existing studies focus on post-implementation periods, observing a general recovery trend characterized by increasing FVC [19,26,53]. However, grassland degradation and restoration are complex processes influenced by interactions between climate change and management practices [54]. By integrating the residual analysis for the pre- and post-implementation periods (i.e., 1980–2000 and 2001–2020)

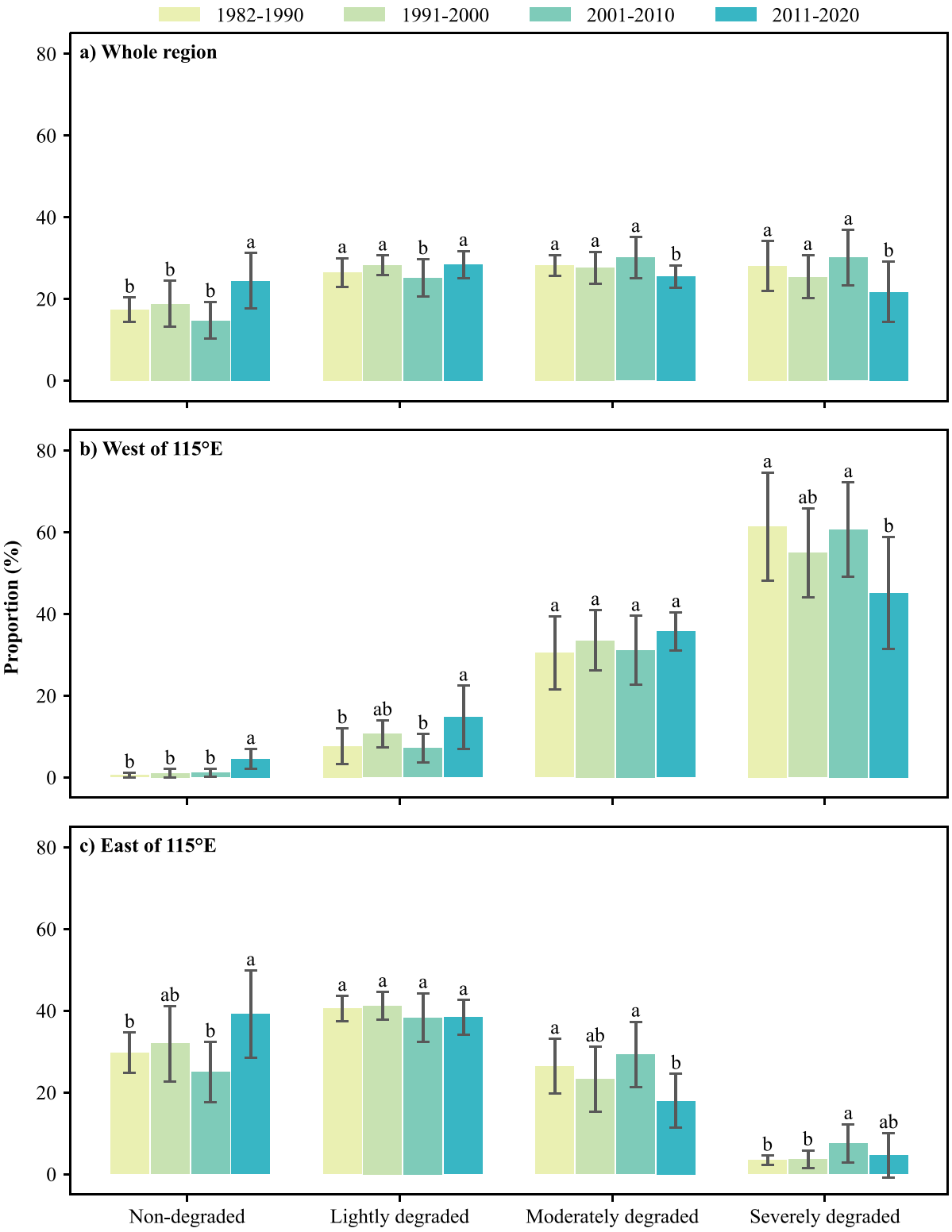

Fig. 7. Area proportions of the Inner Mongolia grassland at different degradation levels across four time periods: 1982–1990, 1991–2000, 2001–2010 and 2011–2020. (a) The whole grassland, (b) grassland in the west of 115°E, and (c) grassland in the east of 115°E. Bars represent mean values for each period, with error bars indicating standard deviation. Different lowercase letters above bars denote significant differences ($p < 0.05$) between time periods for each degradation level. To determine the proportion of grassland in each degradation level for each period, we utilized a raster image containing 8,472 pixels of the study area for each year. Each pixel holds a corresponding Grassland Degradation Index (GDI) value. Based on these GDI values, we classified degradation levels into four categories: non-degraded ($0.8 \leq GDI \leq 1$), lightly degraded ($0.6 \leq GDI < 0.8$), moderately degraded ($0.4 \leq GDI < 0.6$), and severely degraded ($0 \leq GDI < 0.4$). Next, we calculated the number of pixels in each category and then divided it by the total number of pixels (8,472) to obtain the proportion of each degradation category. Finally, we averaged the proportions of degradation categories for the years included in each period to determine the proportion of grassland in each degradation category within each period.

Table 2
Trends in grassland degradation over the last 4 decades.

Item	Region	1982–2000		2001–2020		1982–2020	
		Slope (% a^{-1})	p	Slope (% a^{-1})	p	Slope (% a^{-1})	p
ND[a]	Whole region	0.15 ± 0.19	> 0.1	0.64 ± 0.26	< 0.05	0.16 ± 0.09	0.07
	West of 115°E	0.06 ± 0.03	0.07	0.30 ± 0.07	< 0.001	0.12 ± 0.02	< 0.001
	East of 115°E	0.22 ± 0.31	> 0.1	0.89 ± 0.41	< 0.05	0.19 ± 0.14	> 0.1
LD[b]	Whole region	0.18 ± 0.12	> 0.1	0.17 ± 0.17	> 0.1	0.01 ± 0.05	> 0.1
	West of 115°E	0.35 ± 0.15	< 0.05	0.55 ± 0.25	< 0.05	0.18 ± 0.08	< 0.05
	East of 115°E	0.06 ± 0.14	> 0.1	−0.09 ± 0.20	> 0.1	−0.10 ± 0.06	> 0.1
MD+SD[c]	Whole region	−0.33 ± 0.28	> 0.1	−0.81 ± 0.39	< 0.05	−0.18 ± 0.13	> 0.1
	West of 115°E	−0.41 ± 0.18	< 0.05	−0.85 ± 0.31	< 0.05	−0.31 ± 0.10	< 0.01
	East of 115°E	−0.28 ± 0.38	> 0.1	−0.80 ± 0.50	> 0.1	−0.09 ± 0.16	> 0.1

Note: Slope values indicate the mean ± standard error. [a]Proportion of non-degraded grassland (%). [b] Proportion of lightly degraded grassland (%). [c] Total proportion of moderately and severely degraded grasslands (%).

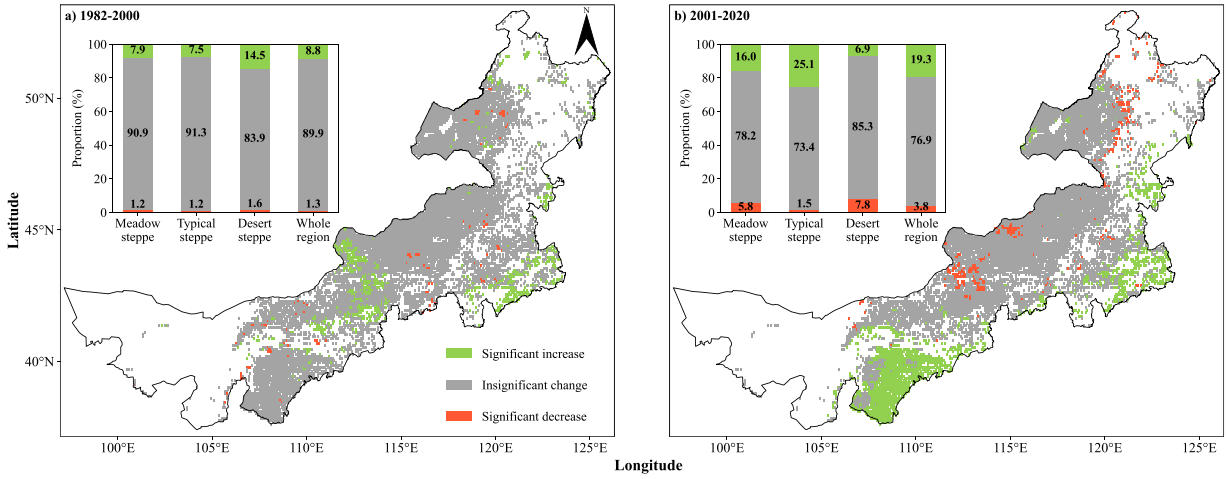

Fig. 8. Significance spatial distribution of fractional vegetation cover (FVC) residue trend in the Inner Mongolia grassland. (a) 1982–2000 and (b) 2001–2020. The significance level was set at a threshold of 0.05. Inset figures show the proportions of different types of residual trends across different grassland types. The map is based on the standard map with approval number GS (2024) 0650 from the Ministry of Natural Resources of the People's Republic of China. The base map boundaries remain unmodified.

(Fig. 8a,b), we can effectively isolate the impacts of both climate change and anthropogenic factors. Additionally, for the first time, our analysis incorporates a geographical boundary at 115°E for the study region. This allows us to not only identify distinct spatial trends in grassland degradation but also provide insights for developing region-specific policies that can more effectively promote grassland recovery.

4.1. Relationship between grassland conditions and climate factors

Not only the FVC (Table S3) but also the proportions of LD and ND grasslands (Fig. 7; Table S4) in the west of 115°E were significantly lower than those in the east of 115°E. Note that the MAP over the period 1982–2020 (Fig. S10a) in the west of 115°E (248 ± 42 mm) was significantly lower than that in the east of 115°E (346 ± 55 mm), which agrees with the detrimental impact of reduced precipitation on grassland productivity within temperate grassland ecosystems [55]. Plotting annual FVC in Fig. 2b and c against MAP, the correlation was significant (West of 115°E: $R^2 = 0.55$, $p < 0.001$; East of 115°E: $R^2 = 0.49$, $p < 0.001$; Fig. S11a,b), further suggesting the importance of precipitation in temperate grassland productivity. It is interesting to note that the slopes in both the east and the west of 115°E grasslands were very close, suggesting that the different grassland types in Inner Mongolia (Fig. 1) have similar responses of FVC to MAP. Moreover, a positive correlation of year-to-year changes between FVC and MAP was also observed ($R^2 = 0.48$, $p < 0.001$; Fig. S11c). The mean value of FVC in the period 2001–2010 was significantly lower than those in the periods 1991–2000 and 2011–2020 in the east of 115°E, which is likely attributed to the low MAP (Table S3). No significant correlation between annual FVC and MAT was observed for the grassland in the west or east of 115°E.

4.2. Impacts of ecological protection measures on grassland recovery

The FVC slope-change trend in the southwest region, the southeast region and the western part of the northeast region showed a shift from stable to improving and continuously improving, which can also be supported by the positive FVC residual trend during 2001–2020 (Fig. 8b). This indicates that the ecological projects implemented in these regions had a positive impact on grassland restoration. Particularly in the southwest region, the synergistic effect produced by the joint implementation of multiple ecological projects may have facilitated the recovery of the grassland ecosystem (Fig. S1) [15]. In the central region, on the contrary, despite the implementation of certain ecological protection measures (Fig. S1), the recovery trend observed during 1982–2000 was not maintained (Fig. 5), and even a negative FVC residual trend emerged during 2001–2020 (Fig. 8b). These regions are experiencing more intensive human activities such as coal mining, which can certainly compromise or even offset the impacts of ecological protection measures [56]. In the eastern part of the northeast region, which is characterized by relatively humid climatic conditions (Supplemental Fig. S10), temperature has become the primary limiting factor, and lower temperature in this region may suppress grassland growth [53]. Moreover, the negative FVC residual trend and the shift in the slope-change trend from stable to deteriorating indicate potential overexploitation of grassland resources in this area. Li et al. [57] also found that population growth,

road construction, and industrial expansion in this region can exert negative impacts on the grassland ecological environment.

The promoting effects of ecological protection on grassland restoration can also be demonstrated by the significant recovery rate of degraded grassland in the last two decades (2001–2020) (Table 2). Note that the proportion of ND grassland increased at a rate of 0.89% a^{-1} in the east of 115°E, approximately 3-fold higher than that in the west of 115°E (Table 2). When the slope of ND grassland in the last two decades (Table 2) was correlated with the corresponding MAP, the correlation was significant (Slope = 0.0076 × MAP–1.608, R^2 = 1.00, n = 3), suggesting that the precipitation may amplify the effect of ecological protection on grassland restoration [58]. Furthermore, a wetter climate is likely to promote the self-recovery capability of grassland [25], which may partly explain why the total proportion of the MD and SD grasslands in the east of 115°E (29.0% ± 11.3%) is much lower than that in the west of 115°E (88.2% ± 7.6%) over the period 1982–2020. Although the decrease in the total proportion of MD and SD grasslands in the west of 115°E is obvious (Table 2), the situation of grassland degradation is currently serious (Fig. 6b), with 80.8% ± 9.9% of the grassland suffering from severe and moderate degradation. Considering that the effect of ecological protection, such as grazing exclusion on the recovery of LD grassland was not significant [59,60], the central government and/or the local government should pay special attention to mitigating the degradation and promoting the recovery of the degraded grassland in the west of 115°E via further implementation of ecological restoration measures.

4.3. Policy implications for grassland management

Based on the above analysis, we urge policymakers at both central and local governments to design geographically and environmentally specific grassland management policies. These policies should address the unique challenges faced by each region. For instance, in regions with initial restoration success (i.e., the southwest and southeast regions), successful experiences should be documented, and project plans should be further refined to promote continuous grassland restoration. This is especially crucial in the arid areas west of 115°E, where scarce precipitation limits natural recovery, making the process slow if relying solely on natural recovery [3]. In the central mining regions experiencing significant human disturbance, stricter enforcement of ecological protection measures and limitations on excessive mining activities are essential to prevent further grassland degradation. The northeast meadow steppe, though experiencing less severe degradation due to overexploitation, still requires effective measures. These may include strengthening law enforcement, and expanding the area of fencing and grazing prohibition, to curb the degradation trend of grasslands and achieve sustainable utilization of grassland resources.

4.4. Limitations and prospects

Several limitations and future directions should be noted in interpreting our results. Firstly, while fractional vegetation cover (FVC) is a valuable tool for assessing grassland degradation, it is just one piece of the puzzle. Future studies should incorporate additional ecological indicators like native species composition, plant height, aboveground biomass, and soil quality [3,31] to provide a more comprehensive understanding of grassland health and complex ecological processes. Secondly, although previous studies have validated the MODIS and GIMMS NDVI-derived FVC products [61], and our study shows consistency between them, future direct field observations and validation specific to our study area would strengthen our findings. Thirdly, while our analysis primarily focused on changes in FVC per pixel, the potential impacts of land use changes on grassland area were not explicitly addressed in our main analysis. Although the CLCD data [62] indicate that the total grassland area remained relatively stable during the study period (Fig. S12; Table S6), suggesting that the temporal variation in land cover during the study period had limited impact on our conclusions, it is important to acknowledge that ecosystem type may change in certain pixels in the future, potentially resulting in irreversible ecological disasters, such as the transition from grassland to desert. Future research could benefit from a more detailed integration of land use change data to account for any localized conversions between grassland and other land use types. Finally, while we show a slowdown in Inner Mongolia grassland degradation (Figs. 6, 7; Tables 2, S4), there is a lack of spatiotemporal data regarding specific ecological restoration measures implemented (e.g., grazing exclusion zones, native species planting). Further investigation should integrate such data to quantify the effectiveness of these restoration efforts in promoting grassland recovery.

5. Conclusion

The fractional vegetation cover (FVC) in the Inner Mongolia grassland shows significant spatial differences. The grassland with low FVC is distributed in the west of 115°E, while that with high FVC predominates in the east of 115°E. The FVC has generally increased over the past four decades, especially in the last two decades (2001–2020). Consistent with the FVC changes, the total proportion of moderately degraded and severely degraded grasslands has decreased, and that of the non-degraded (ND) grassland has increased significantly. The increase in ND grassland area in the east of 115°E is more pronounced than that in the west of 115°E, depending on the mean annual precipitation. The implementation of ecological protection in Inner Mongolia has slowed down grassland degradation, while the situation of grassland degradation is still serious, particularly in the west of 115°E, where 80.8% of the grassland was moderately and severely degraded in the last decade. The central government and/or the local government should pay more attention to retarding the degradation and promoting the recovery of the degraded grassland in the west of 115°E.

Declaration of competing interest

The authors declare that they have no conflicts of interest in this work.

Acknowledgments

This work was jointly supported by the National Natural Science Foundation of China (42375116 and 42171293) and the Fundamental Research Funds for the Central Universities.

Supplementary materials

Supplementary material associated with this article can be found, in the online version, at doi:10.1016/j.fmre.2024.10.006.

References

[1] F.P. O'Mara, The role of grasslands in food security and climate change, Ann. Bot. 110 (6) (2012) 1263–1270.
[2] R.D. Bardgett, J.M. Bullock, S. Lavorel, et al., Combatting global grassland degradation, Nat. Rev. Earth Environ. 2 (10) (2021) 720–735.
[3] Q. Pan, J. Sun, Y. Yang, et al., Issues and solutions on grassland restoration and conservation in China, Bull. Chin. Acad. Sci. 36 (6) (2021) 666–674.
[4] C. Li, R. de Jong, B. Schmid, et al., Changes in grassland cover and in its spatial heterogeneity indicate degradation on the Qinghai-Tibetan Plateau, Ecol. Indic. 119 (2020) 106641.
[5] P. Dlamini, P. Chivenge, A. Manson, et al., Land degradation impact on soil organic carbon and nitrogen stocks of sub-tropical humid grasslands in South Africa, Geoderma 235 (2014) 372–381.
[6] C. Gang, W. Zhou, Y. Chen, et al., Quantitative assessment of the contributions of climate change and human activities on global grassland degradation, Environ. Earth Sci. 72 (2014) 4273–4282.
[7] T. Akiyama, K. Kawamura, Grassland degradation in China: Methods of monitoring, management and restoration, Grassl. Sci. 53 (1) (2007) 1–17.

[8] Z. Wang, X. Deng, W. Song, et al., What is the main cause of grassland degradation? A case study of grassland ecosystem service in the middle-south Inner Mongolia, Catena 150 (2017) 100–107.
[9] K. Phukubye, M. Mutema, N. Buthelezi, et al., On the impact of grassland management on soil carbon stocks: A worldwide meta-analysis, Geoderma Reg. 28 (2022) e00479.
[10] K.G. Lyons, P. Török, J.-M. Hermann, et al., Challenges and opportunities for grassland restoration: A global perspective of best practices in the era of climate change, Glob. Ecol. Conserv. (2023) e02612.
[11] D. Xiong, P. Shi, X. Zhang, et al., Effects of grazing exclusion on carbon sequestration and plant diversity in grasslands of China—a meta-analysis, Ecol. Eng. 94 (2016) 647–655.
[12] L. Wang, Y. Gan, M. Wiesmeier, et al., Grazing exclusion—an effective approach for naturally restoring degraded grasslands in Northern China, Land Degrad. Dev. 29 (12) (2018) 4439–4456.
[13] L. Li, J. Chen, X. Han, et al., Grassland Ecosystems of China, 1st edn, Springer, Singapore, 2020.
[14] L. Hou, F. Xia, Q. Chen, et al., Grassland ecological compensation policy in China improves grassland quality and increases herders' income, Nat. Commun. 12 (1) (2021) 4683.
[15] Q. Shao, S. Liu, J. Ning, et al., Assessment of ecological benefits of key national ecological projects in China in 2000-2019 using remote sensing, Acta Geogr. Sin. 77 (2022) 2133–2153.
[16] Y. Huang, W. Sun, Z. Qin, et al., The role of China's terrestrial carbon sequestration 2010–2060 in offsetting energy-related CO_2 emissions, Natl. Sci. Rev. 9 (8) (2022) nwac057.
[17] Z. Wang, G. Han, X. Hao, et al., Effect of manipulating animal stocking rate on the carbon storage capacity in a degraded desert steppe, Ecol. Res. 32 (2017) 1001–1009.
[18] R. Zhang, Z. Wang, G. Han, et al., Grazing induced changes in plant diversity is a critical factor controlling grassland productivity in the Desert Steppe, Northern China, Agric. Ecosyst. Environ. 265 (2018) 73–83.
[19] H. Zhang, X. Yang, D. Yang, et al., Spatio-temporal changes in grassland fractional vegetation cover in Inner Mongolia from 2000 to 2020 and a future forecast, Acta Pratacult Sin. 32 (8) (2023) 1.
[20] N. Zhu, H. Wang, X. Ning, et al., Advances in remote sensing monitoring of grassland degradation, Sci. Surv. Map 46 (05) (2021) 66–76.
[21] T. Purevdorj, R. Tateishi, T. Ishiyama, et al., Relationships between percent vegetation cover and vegetation indices, Int. J. Remote Sens. 19 (18) (1998) 3519–3535.
[22] A.A. Gitelson, Y.J. Kaufman, R. Stark, et al., Novel algorithms for remote estimation of vegetation fraction, Remote Sens. Environ. 80 (1) (2002) 76–87.
[23] M. Zhumanova, C. Mönnig, C. Hergarten, et al., Assessment of vegetation degradation in mountainous pastures of the Western Tien-Shan, Kyrgyzstan, using eMODIS NDVI, Ecol Indic 95 (2018) 527–543.
[24] Q. Gao, Y.e. Li, Y. Wan, et al., Grassland degradation in Northern Tibet based on remote sensing data, J Geogr Sci 16 (2006) 165–173.
[25] F. Sun, W. Sun, Y. Huang, et al., Precipitation does not amplify the efficiency of fencing measures for temperate grassland restoration: A case study in northern China based on remote sensing, Ecol. Eng. 105 (2017) 252–261.
[26] Z. Xue, M. Kappas, D. Wyss, Spatio-temporal grassland development in Inner Mongolia after implementation of the first comprehensive nation-wide grassland conservation program, Land 10 (1) (2021) 38.
[27] J. Fang, X. Geng, X. Zhao, et al., How many areas of grasslands are there in China? Sci. Bull. 63 (17) (2018) 1737–1739.
[28] Z. Liao, K. Su, X. Jiang, et al., Spatiotemporal variation and coupling of grazing intensity and ecosystem based on four quadrant model on the Inner Mongolia, Ecol Indic 152 (2023) 110379.
[29] G. Wang, Z. Luo, Y. Huang, et al., Preseason heat requirement and days of precipitation jointly regulate plant phenological variations in Inner Mongolian grassland, Agr. Forest Meteorol. 314 (2022) 108783.
[30] H. Chen, L. Shao, M. Zhao, et al., Grassland conservation programs, vegetation rehabilitation and spatial dependency in Inner Mongolia, China, Land Use Policy 64 (2017) 429–439.
[31] B. Li, The rangeland degradation in North China and its preventive strategy, Sci. Agric. Sin. 30 (1997) 1–9.
[32] J.E. Pinzon, C.J. Tucker, A non-stationary 1981–2012 AVHRR NDVI3g time series, Remote Sens. 6 (8) (2014) 6929–6960.
[33] C.J. Tucker, J.E. Pinzon, M.E. Brown, et al., An extended AVHRR 8-km NDVI dataset compatible with MODIS and SPOT vegetation NDVI data, Int. J. Remote Sens. 26 (20) (2005) 4485–4498.
[34] K. Didan, MODIS/Terra vegetation indices 16-day L3 global 1 km SIN grid V061, 2021. https://doi.org/10.5067/MODIS/MOD13A2.061.
[35] A. Huete, K. Didan, T. Miura, et al., Overview of the radiometric and biophysical performance of the MODIS vegetation indices, Remote Sens. Environ. 83 (1–2) (2002) 195–213.
[36] B.N. Holben, Characteristics of maximum-value composite images from temporal AVHRR data, Int. J. Remote Sens. 7 (11) (1986) 1417–1434.
[37] Y. Ding, S. Peng, Spatiotemporal trends and attribution of drought across China from 1901 to 2100, Sustain 12 (2) (2020) 477.
[38] S.E. Fick, R.J. Hijmans, WorldClim 2: New 1-km spatial resolution climate surfaces for global land areas, Int. J. Climatol. 37 (12) (2017) 4302–4315.
[39] Y.X. Zhu, Y.J. Zhang, J.X. Zu, et al., Performance evaluation of GIMMS NDVI based on MODIS NDVI and SPOT NDVI data, J. Appl. Ecol. 30 (2) (2019) 536–544.
[40] D. Mao, Z. Wang, L. Luo, et al., Integrating AVHRR and MODIS data to monitor NDVI changes and their relationships with climatic parameters in Northeast China, Int. J. Appl. Earth Obs. 18 (2012) 528–536.
[41] G. Gutman, A. Ignatov, The derivation of the green vegetation fraction from NOAA/AVHRR data for use in numerical weather prediction models, Int. J. Remote Sens. 19 (8) (1998) 1533–1543.
[42] C. Liu, X. Zhang, T. Wang, et al., Detection of vegetation coverage changes in the Yellow River Basin from 2003 to 2020, Ecol. Indic. 138 (2022) 108818.
[43] X. He, F. Zhang, Y. Cai, et al., Spatio-temporal changes in fractional vegetation cover and the driving forces during 2001–2020 in the northern slopes of the Tianshan Mountains, China, Environ. Sci. Pollut. Res. (2023) 1–21.
[44] Y. Yang, T. Wu, S. Wang, et al., Fractional evergreen forest cover mapping by MODIS time-series FEVC-CV methods at sub-pixel scales, ISPRS J. Photogramm Remote Sens. 163 (2020) 272–283.
[45] P.K. Sen, Estimates of the regression coefficient based on Kendall's tau, J. Am. Stat. Assoc. 63 (324) (1968) 1379–1389.
[46] Y. Wei, S. Sun, D. Liang, et al., Spatial–temporal variations of NDVI and its response to climate in China from 2001 to 2020, Int. J. Digit. Earth 15 (1) (2022) 1463–1484.
[47] M.G. Kendall, Rank Correlation Methods, 1st edn, Charles Griffin, London, 1948.
[48] K.H. Hamed, Trend detection in hydrologic data: The Mann–Kendall trend test under the scaling hypothesis, J. Hydrol. 349 (3–4) (2008) 350–363.
[49] R.S. Lovell, S. Collins, S.H. Martin, et al., Space-for-time substitutions in climate change ecology and evolution, Biol. Rev. 98 (6) (2023) 2243–2270.
[50] S.T. Pickett, Space-for-time substitution as an alternative to long-term studies, in: Long-term Studies in Ecology: Approaches and Alternatives, Springer, New York, 1989, pp. 110–135.
[51] M. Wiesmair, H. Feilhauer, A. Magiera, et al., Estimating vegetation cover from high--resolution satellite data to assess grassland degradation in the Georgian Caucasus, Mt. Res. Dev. 36 (1) (2016) 56–65.
[52] J. Evans, R. Geerken, Discrimination between climate and human-induced dryland degradation, J. Arid. Environ. 57 (4) (2004) 535–554.
[53] S. Mu, H. Yang, J. Li, et al., Spatio-temporal dynamics of vegetation coverage and its relationship with climate factors in Inner Mongolia, China, J. Geogr. Sci. 23 (2013) 231–246.
[54] Z. Yan, Z. Gao, B. Sun, et al., Global degradation trends of grassland and their driving factors since 2000, Int. J. Digit. Earth 16 (1) (2023) 1661–1684.
[55] D.A. Frank, Drought effects on above-and belowground production of a grazed temperate grassland ecosystem, Oecologia 152 (1) (2007) 131–139.
[56] X. Dong, B. Yu, M. Brown, et al., Environmental and economic consequences of the overexploitation of natural capital and ecosystem services in Xilinguole League, China, Energy Policy 67 (2014) 767–780.
[57] J. Li, Q. Liu, P. Liu, Spatio-temporal changes and driving forces of fraction of vegetation coverage in Hulunbuir (1998-2018), Acta Ecol. Sin. 42 (1) (2022) 220–235.
[58] L. Hao, G. Sun, Y. Liu, et al., Effects of precipitation on grassland ecosystem restoration under grazing exclusion in Inner Mongolia, China, Landsc. Ecol. 29 (2014) 1657–1673.
[59] X. Wang, Q. Ge, X. Geng, et al., Unintended consequences of combating desertification in China, Nat Commun 14 (1) (2023) 1139.
[60] N. Zong, P. Shi, L. Zheng, et al., Restoration effects of fertilization and grazing exclusion on different degraded alpine grasslands: Evidence from a 10-year experiment, Ecol. Eng. 170 (2021) 106361.
[61] D. Wu, H. Wu, X. Zhao, et al., Evaluation of spatiotemporal variations of global fractional vegetation cover based on GIMMS NDVI data from 1982 to 2011, Remote Sens. 6 (5) (2014) 4217–4239.
[62] J. Yang, X. Huang, The 30m annual land cover dataset and its dynamics in China from 1990 to 2019, Earth Syst. Sci. Data 13 (8) (2021) 3907–3925.

Haojun Zheng is currently a Ph.D. candidate at the Institute of Atmospheric Physics, Chinese Academy of Sciences. He obtained his bachelor's degree from Chongqing University in 2021. His research interests focus on soil organic carbon and grassland ecology.

Guocheng Wang (BRID:03.193.00.02163) is a research scientist and a doctoral advisor at Beijing Normal University, specializing in soil organic carbon, sustainable agriculture, and grassland ecology. He is leading the development of an agroecosystem model (i.e., AgroC-R) to improve understanding of agricultural systems and contribute to national greenhouse gas inventories. His work also focuses on creating efficient methods to predict the best strategies for stable crop production, soil carbon sequestration, and greenhouse gas emission reduction at large scales. He is also investigating how carbon stocks in northern China's grasslands are impacted by the changing climate and ecological protection measures.